Topology and pressure distribution reconstruction of an englacial channel

Laura Piho[1,*], **Andreas Alexander**[2,3,*], **Maarja Kruusmaa**[1,4]

[1]Centre for Biorobotics, Tallinn University of Technology
[2]Department of Geosciences, University of Oslo
[3]Department of Arctic Geology, The University Centre in Svalbard
[4]Centre for Autonomous Marine Operations and Systems, Norwegian University of Science and Technology
[*]Shared co-first authorship

Key Points:

- We present a method to reconstruct subsurface water flows from *in situ* measurements with sensing drifters
- We showcase the method with the reconstruction of the flow path and the spatial water pressure distribution of an englacial channel
- Our methods opens up new ways to study en- and subglacial drainage systems and other subsurface fluid flow paths

Corresponding author: Andreas Alexander, andreas.alexander@geo.uio.no

Abstract

Glacial hydrology describes the way water moves over, through and under glaciers. Meltwater flows every summer over the surface of glaciers and ice sheets, creating pathways down to below the surface, eventually reaching the glacier bed and thereby influencing ice motion. Glacier and ice sheet models, trying to predict their future sea-level rise contribution, need to therefore be able to properly describe glacial hydrological processes. However, the current knowledge in the field is still limited due to the lack of measurement technology for subsurface *in situ* flow observations. Here we present a measurement method that allows to reconstruct planar subsurface water flow paths and spatially reference water pressures therein. The approach uses inertial measurements from submersible sensing drifters and reconstructs the flow path from given start and end coordinates. Validation cases show an average error of 3.90 m compared to GNSS reference. We showcase this method by reconstructing the flow path and the spatial water pressure distribution of an englacial channel on Austre Brøggerbreen (Svalbard). The average error of the reconstruction is thereby 12.1 m and the average pressure error 3.4 mbar (0.3%). Our method will allow to study en- and subglacial flow paths and the pressure distribution therein, thereby allowing for model validation and activation. Further on, our method also allows to reconstruct other subsurface fluid flow paths, when a global spatial reference (e.g. GNSS) is not available.

Plain Language Summary

The imprecision of glacier and ice sheets models is a major contributor to the uncertainty of future sea level rise predictions. This uncertainty is partly caused by the lack of *in situ* observations from subsurface hydrology where simultaneous records of subsurface water flow paths and the pressures within are highly relevant. We present a method to reconstruct subsurface flow paths from inertia sensing drifter measurements and align readings of pressure sensors to them. Our results open up new ways to measure in previously inaccessible environments and can thus contribute data, not only for model validation and calibration, but also for model activation.

1 Introduction

Predictions about future sea-level rise are uncertain, as outlined in the recent IPCC report (Pörtner et al., 2019). The uncertainty rises partly from our incomplete understanding of glacier and ice sheet dynamics, where glacier hydrology plays a key role. Our incomplete knowledge of glacier hydrology is mostly caused by lack of direct observations of the en- and subglacial environment, making it hard to constrain, yet verify theoretical and numerical models (Hooke, 1989; Flowers, 2015a, 2015b). Even though hydrological glacier models have made tremendous progress in the recent years, their calibration still remains difficult (Flowers, 2015a).

Water can generally transit through and under glaciers and ice sheets in en- and subglacial drainage systems. The physical configuration of these drainage systems varies between individual glaciers and ice sheets, as well as on spatial and temporal scale (Hubbard & Nienow, 1997; Fountain & Walder, 1998). Even the most sophisticated hydrological models, simulating the behavior of the hydrological system and linking it to ice dynamics, employ the basic concepts of hydraulic potentials (Shreve, 1972) and the physical principles laid out by Röthlisberger (Röthlisberger, 1972) almost 50 years ago (see Flowers (2015a) for a review of current models). The theory of hydraulic potential is thereby utilizing glacier geometry to calculate hypothetical water pathways (Shreve, 1972; Björnsson, 1975). Fluxes are often expressed empirically as a function of the hydraulic potential, where several parameters need

to be determined empirically by the modeler (Flowers, 2015a). The lack of direct observations makes it thereby hard to validate the choice of model parameters, thus contributing to the uncertainty of the models.

Over the years, a broad spectrum of methods for studying inaccessible subsurface flows has been developed in glaciology. Typical empirical research approaches for temperate alpine glaciers include: investigations of bulk meltwater discharge and chemistry, tracer studies, proglacial bedrock investigations and borehole measurements (Hubbard & Nienow, 1997). These techniques are, with the exemption of the last one, indirect methods, thus not allowing direct measurements of the subsurface environment. Previous years have seen the use of time-consuming geophysical investigation methods, utilizing ground penetrating radar (GPR) (e.g., Stuart et al., 2003; Bælum & Benn, 2011; Hansen et al., 2020; Schaap et al., 2020) and seismic arrays (Gimbert et al., 2016; Nanni et al., 2020) to locate en- and subglacial channels. In wintertime, moulins and meltwater channels are accessible for direct speleological investigations and mapping of water flow paths in shallow glaciers (e.g., Holmlund, 1988; Vatne, 2001; Gulley et al., 2009; Alexander, Obu, et al., 2020; Hansen et al., 2020). Water pressures have been indirectly induced from geophysical models utilizing seismic arrays (Nanni et al., 2020) or directly measured via moulins and boreholes (e.g., Iken, 1972; Iken & Bindschadler, 1986; Engelhardt et al., 1990; Hubbard et al., 1995; Stone & Clarke, 1996; Vieli et al., 2004; Andrews et al., 2014). The latter is, however, point-scale by nature (Flowers, 2015a). Therefore the development of new remote sensing methods for direct measurements of basal drainage parameters over spatial scales is a top research priority to reduce uncertainty of glacier and ice sheet models (Flowers, 2015a, 2015b).

In recent years submersible drifters have been proposed to measure water pressures along the flow path of glacial drainage systems (Bagshaw et al., 2012, 2014; Alexander, Kruusmaa, et al., 2020). Since the subsurface environments are GPS denied, the recorded data of these platforms lack spatial reference. Previously we have proposed the use of inertial measurement units (IMUs), containing accelerometers, gyroscopes and magnetometers, alongside pressure recordings and demonstrated high repeatability of measurements in a supraglacial channel(Alexander, Kruusmaa, et al., 2020). In theory, double integration of the recorded acceleration data would result in travelled distance. In practice, error accumulation and noise lead to high uncertainty. This is a familiar problem in navigation, known as a dead reckoning error (Montello, 2005). The double integration error in dead-reckoning grows linearly if the acceleration offset is small but for a significant acceleration offset, the error can grow quadratically and very quickly lead to high uncertainty. In mobile robotics this problem is commonly addressed using probabilistic mapping, localization and navigation algorithms (Thrun et al., 1998). Uncertainty is further reduced by using salient features, recognizable by robotic sensors, as landmarks (Thrun, 1998).

In this study we use machine-learning extracted features from IMU data as salient features. The idea for feature extraction is derived from (Fourati et al., 2013), showing that inertial measurement data can be used to map human movement, as human steps have repeated recognizable periods during which the velocity and acceleration are zero. In our previous study (Alexander, Kruusmaa, et al., 2020) we observed distinct signal patterns related to morphology of glacial channels but could not quantify and classify them to extract salient flow features. In this study, we propose to solve this problem using an infinite hidden Markov model giving the probability distribution of features from IMU data. We further propose piece-wise integration of this data to compute the flow path between the extracted features. As such, the accumulated integration errors do not grow unbounded. As result, we obtain a probabilistic track of the channel between two known globally referenced points (e.g. GNSS referenced deployment and recovery points). Measuring pressure

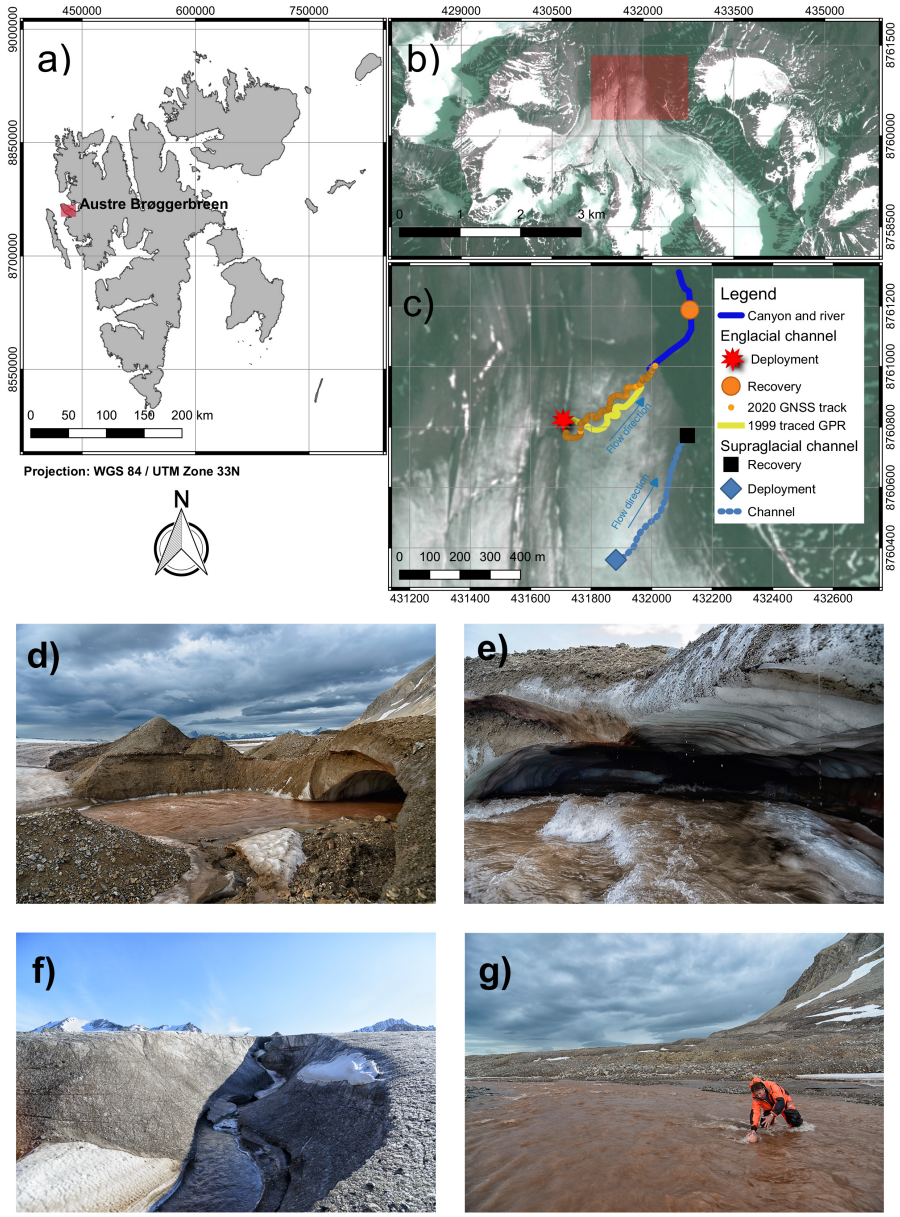

Figure 1: The test site. (a) Location of Austre Brøggerbreen on the Svalbard archipelago. (b) Location of the investigated supra- and englacial channel on the glacier. Background image: Planet Labs, 09.07.2019 (Team Planet, 2017). (c) Map of the studied supra- and englacial channel with flow directions (blue arrows). Shown are the 2019 GNSS track with deployment and recovery point for the supraglacial channel, the 1999 GPR track of the englacial channel from (Stuart et al., 2003), the 2020 GNSS track of the melted out englacial channel, as well as river and canyon section following the englacial channel, mapped out from Planet optical imagery (Team Planet, 2017). Additionally shown are the deployment and recovery points used for drifter deployments at the englacial channel. Background image: Planet Labs, 09.07.2019 (Team Planet, 2017). (d) Deployment point at the englacial channel in 2019. (e) Entrance to the englacial channel in July 2019. (f) Canyon following the outlet of the englacial channel in July 2019. (g) Drifter recovery at the proglacial river in July 2019.

along with the IMU data, further allows to spatially reference the pressure distribution along this track.

We showcase the feasibility and applicability of our approach with the reconstruction of the spatially referenced flow path and the water pressure distribution of an englacial channel on Austre Brøggerbreen (Svalbard, Norwegian Arctic; see also fig. 1). Our reconstructions are based on data collected by a submersible drifter platform containing an IMU as well as pressure sensors and compared to GNSS data gathered by a GNSS surface drifter. The results are validated by the reconstruction of a known rectangular path with respect to dGPS and GNSS reference, as well as with reconstruction of a supraglacial channel (fig. 1(c)) with respect to GNSS reference. We further qualitatively compare our englacial reconstruction to the results of an earlier GPR investigation (Stuart et al., 2003), satellite imagery, as well as to a GNSS reference recorded after the englacial channel had melted out a year later (table 1).

2 Materials and Methods

2.1 Drifter platforms

Two different drifter platforms were used in this study: A submersible drifter for path reconstruction and a GNSS surface drifter for reference measurements.

A detailed description of the submersible drifter can be found in (Alexander, Kruusmaa, et al., 2020). The device is a 12 cm long, 4 cm diameter and 143 g heavy, neutrally buoyant tube (see fig. 2(a)-2(d)). It contains three 2 bar pressure sensors (MS5837-2BA, TE Connectivity, Switzerland) with a sensitivity of 0.02 mbar and a 9 degree of freedom (DOF) IMU (BNO055, Bosch Sensortec, Germany). The sampling rate for the pressure sensors and the IMU is 100 Hz. All data is stored at a 16 GB microSD card in hex format.

The GNSS surface drifter, described in more detail in (Tuhtan et al., 2020) and (Alexander et al., n.d.), served as reference. It is a 0.35 kg heavy, positively buoyant drifter consisting of a 25 cm diameter foam floater enclosing a waterproof box (see fig. 2(e)-2(h)). Inside the box is a custom-built printed circuit board (PCB) containing a Bosch BNO055 IMU and a NEO-M8T GNSS receiver powered by two rechargeable lithium batteries (type 1865, 3.7 V, 3600 mAh). All measurements are stored to a 8GB microSD card at a sampling rate of 5 Hz. The static positioning accuracy of the GNSS is ± 3 m in the horizontal and ± 10 m in the vertical direction (Tuhtan et al., 2020).

2.2 Study site and fieldwork

The fieldwork was conducted on Austre Brøggerbreen, an approximately 5 km long valley glacier, located outside the research settlement Ny-Ålesund on the Norwegian administrated Svalbard archipelago. The glacier has several englacial channels, which have been studied and described regularly over the past 20 years (Vatne, 2001; Stuart et al., 2003; Vatne & Irvine-Fynn, 2016; Kamintzis et al., 2018). Our fieldwork focused on the lower englacial channel, which was mapped 20 years earlier and described in (Vatne, 2001; Stuart et al., 2003). Two different drifter platforms (GNSS surface drifters (Tuhtan et al., 2020) and submersible drifters (Alexander, Kruusmaa, et al., 2020)) were deployed from a former moulin marked with a red star on the map in figure 1(c) between 30.06.2019 and 05.07.2019 during the period of the main spring snow melt. In total we deployed the submersible drifters 24 times. All drifters were recovered by hand from the river in the glacier forefield (orange circle on the map in figure 1(c)), using survival suits. Data was downloaded to a field

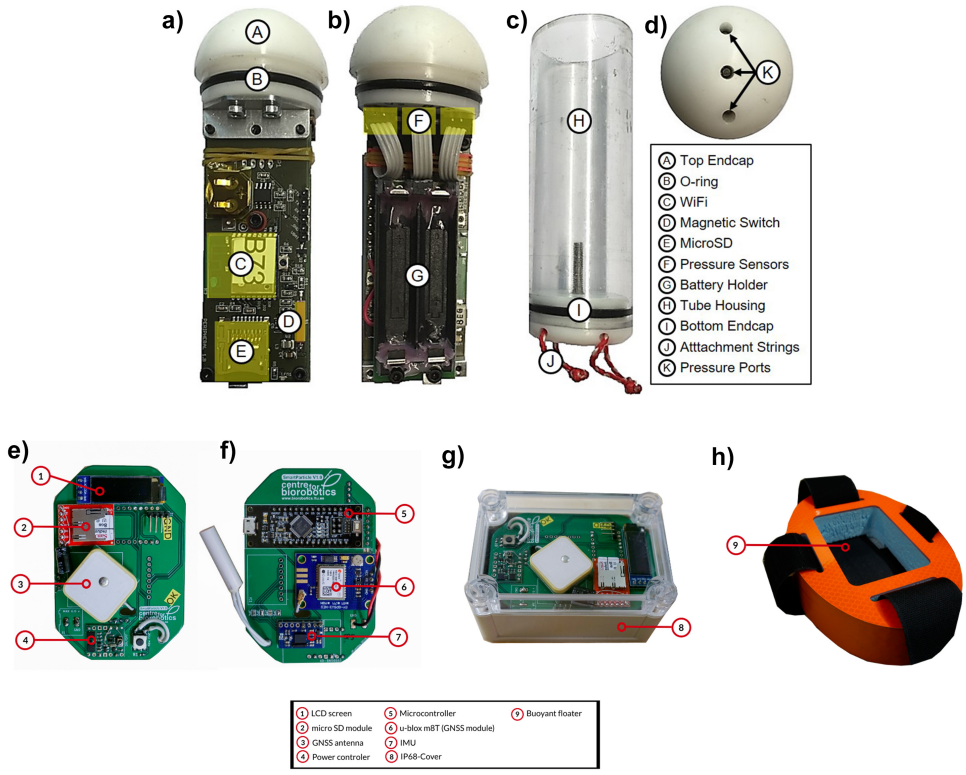

Figure 2: Two different drifter platforms have been used in this study: A submersible drifter and a GNSS surface drifter. (a)-(d) show the submersible drifter and (e)-(h) the GNSS surface drifter. (a) Side view showing the submersible drifter electronics. (b) Side view showing the reverse side of the electronics board including the battery holder and pressure sensors. (c) Polycarbonate tube housing of the submersible drifters with attachment strings for balloons used for manual buoyancy adjustment. (d) Top view facing the cap, showing the ports for each of the three pressure sensors. (e) Side view showing the GNSS surface drifter electronics with LCD screen SD storage, GNSS antenna and power controller. (f) Side view showing the reverse side of the GNSS surface drifter electronics with mirocontroller, GNSS receiver and IMU. (g) The electronics of the GNSS surface drifter are sealed in a waterproof box. (h) The box gets placed at the center of a 30 cm long floater.

computer using WiFi. We revisited the englacial channel on 19.08.2020 and deployed a GNSS enabled surface drifter (Tuhtan et al., 2020) to gather a GNSS path of the now melted-out channel (orange path in fig. 1(c)). We additionally deployed both drifter platforms on a small supraglacial stream further upstream from the englacial channel (shown in light blue in fig. 1(c)) on 02.07.2019.

2.3 Model description

The general workflow of our subsurface flow path reconstruction is shown in figure 3. The input data for the noise removal and feature extraction phases are the gyroscope, acceleration and magnetometer readings of the submersible drifter's inertial measurement unit (IMU). The output of the model is the average flow path in UTM coordinates (WGS84 UTM 32 North) with pressure distribution. The IMUs used (Alexander, Kruusmaa, et al., 2020; Tuhtan et al., 2020) provide internally calculated quaternions as well as Euler angels. For flow path reconstruction additional input is needed to specify the start and end points of the path. In our case those are GPS referenced deployment and recovery coordinates of the drifters. The processing and modeling of data from one deployment took on average 20 minutes. For this, we used MATLAB 2019b on a consumer laptop (1.8 GHz Intel Core i7, 8 GB RAM).

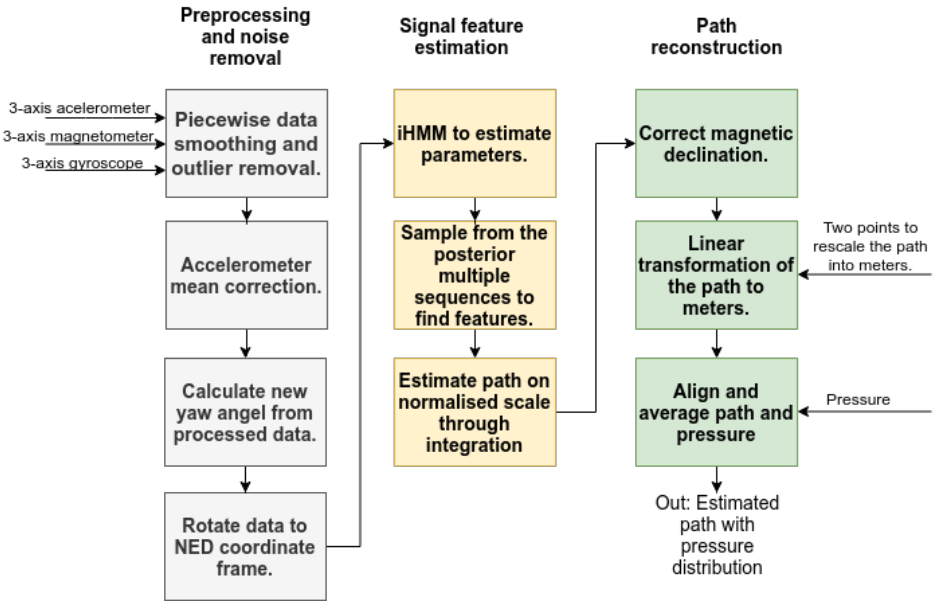

Figure 3: The proposed model workflow diagram. The model applies an infinite hidden Markov model (iHMM) on the IMU data to detect signal features.

2.4 Preprocessing and noise removal

The data from each submersible drifter deployment was manually clipped to only account the time between deployment and recovery. Each deployment dataset consisted thereby of multiple repeated measurements of 9 dof IMU sensor data (3-axis accelerometer, 3-axis magnetometer, and 3-axis gyroscope) at 100 Hz, as well as readings from three pressure sensors.

To obtain an accurate orientation estimation, the IMU data was piecewise filtered and outliers removed. In addition, mean correction was applied to the ac-

celerometer data. The piecewise signal processing was thereby performed by splitting the data up where the mean of the signals changed significantly (Killick et al., 2012). This allowed to subdivide the data and remove noise from each section without oversmoothing the rest of the path. In each section a first order Savitzky-Golay filter (Savitzky & Golay, 1964) was applied to both accelerometer and magnetometer data. We then applied a variance based outlier filter on each section. Abrupt changes in the acceleration behaviour lead to large errors in the rotation calculation and hence considerable jumps in the reconstructed path. To smoothen these jumps we applied a component-wise mean correction on the acceleration data. For this, we calculated the mean along the whole flow path and each individual section. We then calculated the average between the total flow path mean and each section mean and set this average as the new mean for each section.

The data was rotated into earth (NED) reference frame, using the pitch and roll angles from the device and the yaw angel calculated from the processed accelerometer and magnetometer readings. The data was down sampled from 100 Hz to 25 Hz to increase the processing speed of the model.

2.5 Estimating the signal features using infinite hidden Markov model

Hidden Markov models (HMM) are unsupervised learning models in which the state is not fully observable, rather it is only observed indirectly via some noisy observations. In this paper, the noisy observations are the IMU derived accelerometer, magnetometer, and gyroscope signals. Using HMM, the aim is to find the hidden states (features), which are assumed to be associated to the velocity. Similarly to (Fourati et al., 2013), at the beginning of each feature, the velocity is assumed to be zero (or close to zero).

First, consider a finite (regular) HMM that takes the measured IMU signals, denoted by $\mathbf{y} = \{y_1, y_2, ..., y_T\}$ as input (observation sequence), and finds the hidden state sequence $\mathbf{s} = \{s_1, s_2, ..., s_T\}$, which in the scope of this paper is assumed to be the velocity features of the water flow in the channel. In finite HMM, each state takes a value from a finite number of states $1, ..., K$, which have to be predefined. A transition matrix $\boldsymbol{\pi}$ describes the probabilities of moving between states. The probability of moving from state i to state j is given as $\pi_{ij} = p(s_t = i \mid s_{t+1} = j)$ and the initial probabilities are given by $\pi_{0i} = p(s_1 = i)$. In addition, there exists a parameter ϕ_{s_t} for each state $s_t \in \{1, ..., K\}$, that parametrizes the observation likelihood for that state given by $y_t \mid s_t \sim F(\phi_{s_t})$. The observation likelihood describes the probability of an observation y_t being generated from a state. Hence, the HMM can be written as $\{\pi_0, \boldsymbol{\pi}, \boldsymbol{\phi}, K\}$. The joint distribution over hidden states $\mathbf{s}$ and observations $\mathbf{y}$, given the parameters $\{\pi_0, \boldsymbol{\pi}, \boldsymbol{\phi}, K\}$, can be written as:

$$p(\mathbf{s}, \mathbf{y} \mid \pi_0, \boldsymbol{\pi}, \boldsymbol{\phi}, K) = \prod_{t=1}^{T} p(s_t \mid s_{t+1}) p(y_t \mid s_t). \tag{1}$$

The finite HMMs have two big limitations: First, maximum likelihood estimations do not consider the complexity of the model. This makes underfitting and overfitting hard to avoid. Second, the model has to be specified in advance. This means, that even though the hidden states are unknown, the number of different states has to be predefined. Due to the complexity of the model, predefining it is complex, as one has to choose the number of different features in the glacial channels based only on the measured IMU data.

We address these limitations by applying an infinite hidden Markov model (iHMM) (Beal et al., 2002). The iHMM uses Dirichlet processes to define a non-

parametric Bayesian analysis on HMM, allowing countably infinite number of hidden states, thus permitting automatic determination of the number of hidden states. Therefore, not knowing how many different features are present in the glacial channel is not a problem anymore.

In a HMM, the transition matrix $\boldsymbol{\pi}$ is a $K \times K$ matrix, where K is predefined. In iHMM, by contrast $K \to \infty$. To allow this and to complete the Bayesian description, the priors are defined using hierarchical Dirichlet processes (HDP), allowing to have distributions over hyper-parameters and making the model more flexible.

The HDP are a set of DPs coupled through a shared random base measure drawn from a DP. That is, each $G_k \sim \mathrm{DP}(\alpha, G_0)$ with a shared base measure G_0 and a concentration parameter $\alpha > 0$. The shared base measure can be thought of as the mean of G_k and the concentration parameter α controls the variability around G_0. In addition, the shared base measure is also given a DP prior $G_0 \sim \mathrm{DP}(\gamma, H)$, where H is a global base measure. The formal definition of the iHMM is given as:

$$\beta \sim \mathrm{GEM}(\gamma) \tag{2}$$
$$\boldsymbol{\pi}_k \mid \beta \sim \mathrm{DP}(\alpha, \beta) \tag{3}$$
$$\phi_k \sim H \tag{4}$$
$$s_t \mid s_{t-1} \sim \mathrm{Multinomial}(\pi_{s_{t-1}}) \tag{5}$$
$$y_t \mid s_t \sim F(\phi_{s_t}). \tag{6}$$

Where $\mathrm{DP}(\alpha, \beta)$ is a Dirichlet Process, the parameter β is a hyperparameter for the DP that is distributed according to the stick-breaking construction noted as GEM(.) (Sethuraman, 1994). The indicator variable s_t is sampled from the multinomial distribution. Finally, priors are also put on hyperparameters α and γ. As there are no strong beliefs about the hyperparameters, a common practice is to use gamma hyperpriors.

To find the two sets of unknowns, i.e., the hidden states and the hyperparameters, Beam sampling (Van Gael et al., 2008) is used. The Beam sampling combines slice sampling and dynamic programming, where the first limits the number of states considered at each time step to a finite number, and the second samples the hidden states efficiently.

2.6 Path reconstruction

As a result, a posterior probability over sequences of observations has been found, and multiple possible velocity feature (hidden state) sequences are sampled from the posterior distribution. This results in a set of possible sequences of flow features along the glacial water flow path. The path estimation is performed for multiple feature sequences. Hence, creating multiple possible paths and an estimated region of error.

The integration is done in two steps. Assuming that the velocity is zero at the beginning of each feature, the first integration is calculated over each feature separately, setting velocity to zero at the beginning. This results in a velocity profile, that does not correspond to the real velocity values along the path, but describes the changes in velocity along the path. The second integration is performed over the new velocity profile and normalised, resulting in the glacier water flow path topology map on a normalised scale. After correcting magnetic declination, the resulting topology map can be rescaled back to earth coordinates through a linear transformation. This transformation can be found by knowing two distinct points along

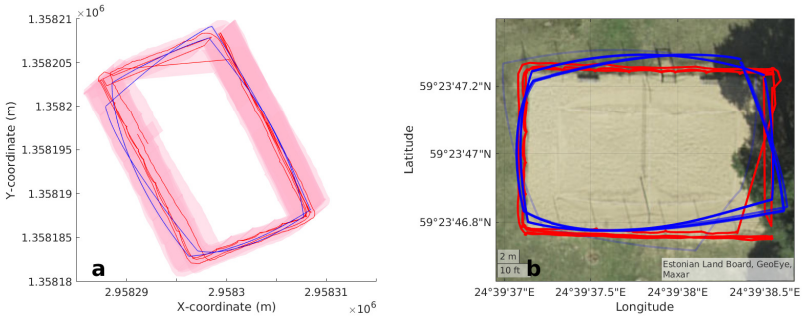

Figure 4: A rectangular volleyball field serves as 'Proof of concept' case.(a) Estimated rectangular path with standard deviations. Blue: The reconstruction. Red: GNSS surface drifter path. All values are given in UTM coordinates.(b) Estimation of the volleyball field with optical satellite image in the background. The reconstruction is shown in blue and the dGPS reference path in red.

Table 1: Overview of the reconstruction cases and the validation methods.

Reconstruction	**Reference for validation**
Rectangular path (volleyball field)	dGPS GNSS surface drifter
Supraglacial channel	GNSS surface drifter
Englacial channel	1999 GPR track 2019 Planet imagery 2020 GNSS surface drifter

the path, in our case, the deployment and recovery positions. The reconstructed paths from each deployment and their pressure distributions are aligned and averaged. The alignment was thereby performed using dynamic time warping (DTW) (Sakoe & Chiba, 1978), such that each subsequent signal was aligned with the mean of previous signals. Overall this resulted in the pressure distribution and estimated average reconstruction of the hydrological flow path.

2.7 Validation cases

To validate our model we used a volleyball field in Tallinn (Estonia) as a first 'proof of concept' case. For this we took two GNSS surface drifters (Tuhtan et al., 2020) and two submersible drifters (Alexander, Kruusmaa, et al., 2020) and walked one round at the outer edge of the field. Additionally we recorded the same track using a Trimble R4 dGPS device.

As second validation case, we used a supraglacial channel on Austre Brøggerbreen (see figure 1(c)), where we deployed both drifter platforms (submersible drifters and GNSS surface drifters) on the 2nd of July 2019 by hand and recovered them further downstream.

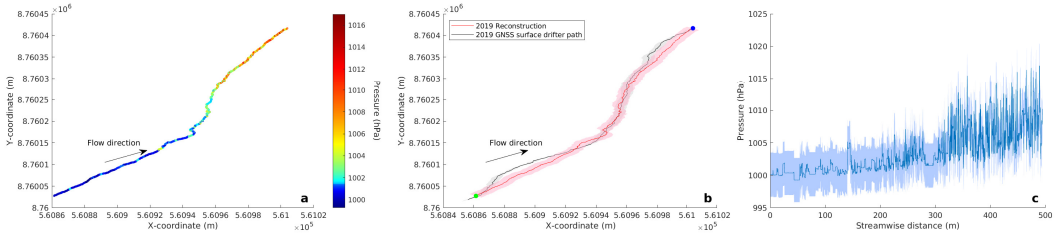

Figure 5: Supraglacial path reconstruction. (a) Reconstructed supraglacial track in UTM coordinates with pressure distribution in hPa. (b) Estimation of the supraglacial track (red) with standard deviations (pink) in UTM coordinates. The GNSS reference is shown in black and the average error of the GNSS recordings in light gray. The deployment and recovery points are denoted with green and blue circles respectively. The arrow denotes the flow direction. (c) Average water pressure with standard deviation along the estimated stream-wise distance of the supraglacial channel.

3 Results

3.1 Known rectangular path

We initially validated our method by the reconstruction of a rectangular path (volleyball field, size 14x23 m) with a known GNSS reference (see figure 4). The path had a total dGPS (Trimbel R4) derived length of 74.0 m. Our reconstruction, based on two IMU datasets, resulted in an average path length of 70.1 m, an underestimation of the real length by -5.3%. We further calculated the position error for each point as

$$Error = \sqrt{(p_x(t) - \hat{p}_x(t))^2 + (p_y(t) - \hat{p}_y(t))^2} \tag{7}$$

where $p_x(t)$ and $p_y(t)$ are the coordinates measured via dGPS and $\hat{p}_x$ and $\hat{p}_y$ are the estimated points from the reconstruction. The resulting average absolute error, based on the 10 nearest points is 0.14 m and the maximum error 2.9 m. This equals an average error of 1% for the width and 0.6% for the length of the rectangle, with maximum errors of 20.7% for the width and 12.6% for the length.

3.2 Supraglacial calibration

We then tested our approach with the reconstruction of a supraglacial channel with known geometry (fig. 1(c)). As a reference, we used an averaged path (see table 1), derived from GNSS surface drifter measurements (Tuhtan et al., 2020). The reconstruction was based on 11 submersible drifter (Alexander, Kruusmaa, et al., 2020) deployments. Our model reproduces a flow path, which is within 3.90 m of the GNSS reference path (figure 5). The lowest error is thereby 2.0 m and the largest deviation from the reference path is 11.10 m, based on the average of 10 nearest points. As fig. 6 shows, the average error from our reconstruction converges after 6 datasets (one drifter deployment needed per dataset). The total length of the GNSS reference track is 449 m, whereas the reconstructed path is 478 m long, equal to an overestimation by 6.5%. The resulting flow path allows further to spatially reference the pressure measurements of the drifters. The obtained pressure distribution map shows pressure variations along the channel with zones of higher pressures occurring mainly in the lower part of the channel and in areas where the channel changes direction.

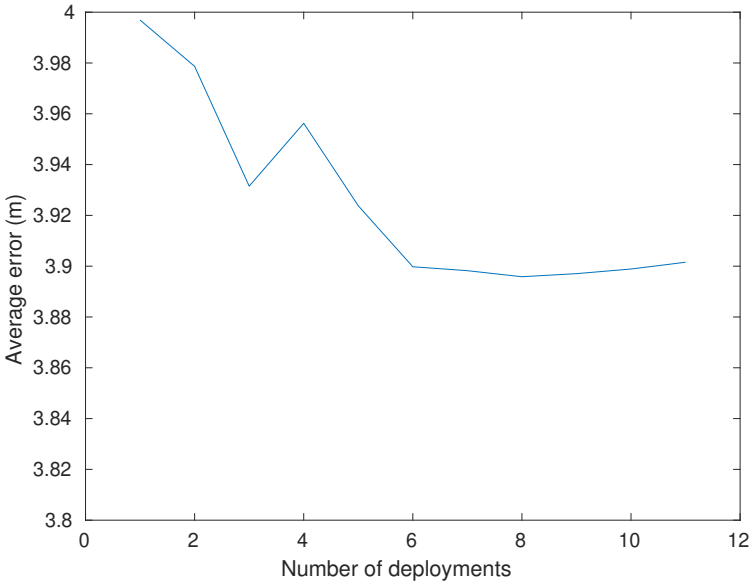

Figure 6: Convergence of the average error for the supraglacial channel reconstruction with respect to the number of deployments.

3.3 Englacial channel reconstruction

The submersible drifter deployments for the reconstruction were collected in July 2019. A revisit of the field site in August 2020 allowed to map the flow path of the channel with the GNSS surface drifter, as the roof of the channel had mostly melted away and transformed the former englacial channel into a deeply incised supraglacial channel, which was only partly ice covered. The reconstruction from the IMU data, collected in 2019 (6 deployments), leads to the mean flow path shown in figure 7(b). The figure also shows the comparison between a GNSS reference track measured a year later in summer 2020 and a GPR measurement from 1999. The shape of the reconstructed flow path thereby resembles the shape of both, the 2020 GNSS reference and the 1999 GPR track from (Stuart et al., 2003).

The overall average position error (based on equation 7) of the reconstructed englacial channel and the proglacial river, compared to the 2020 GNSS reference path for the channel, as well as the 2019 satellite derived proglacial river path (see figure 7), is 12.1 m . The englacial channel part of the reconstruction has an average error of 13.3 m compared to the 2020 GNSS reference (see tab. 1 for an overview of used references). From the englacial outlet through the canyon (fig. 1(f)) and the proglacial river up to the recovery point (fig. 1(g)), the average error of the reconstructed path is 10.9 m compared to the satellite reference path. The path length of the 2020 GNSS reference track (1 deployment) from the englacial channel is 544.8 m. The section after the outlet of the channel through the canyon and the proglacial river measures 290 m on the satellite imagery. Our model returns a total path length of 1027 m from deployment point to recovery point. The channel section is thereby 651 m long and the part through the canyon and the proglacial river 376 m.

The mean pressure recorded by the drifters is 1011.7 mbar with a standard deviation of 3.4 mbar (0.3%). The spatial pressure distribution map (fig. 7(a)) reveals one zone of higher pressure shortly before the englacial channel exits into the open

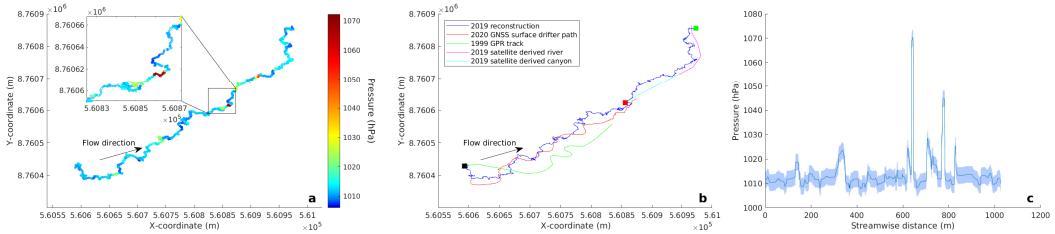

Figure 7: Englacial channel reconstruction. (a) Estimated average track of the englacial channel in UTM coordinates with pressure distribution in hPa. (b) Estimated englacial track in UTM coordinates based on the 2019 IMU data in blue alongside GNSS drifter reference measured in 2020 in red. Further shown are the mapped canyon and proglacial river from optical Planet imagery (acquisition date 09.07.20219, (Team Planet, 2017)), as well as the 1999 GPR map traced from (Stuart et al., 2003). The Black square denotes the deployment point and the green square the recovery location. Additionally shown is the location of the start of the canyon at the end of the englacial channel (red square). (c) Average water pressure with standard deviation along the estimated stream-wise distance of the englacial channel.

canyon. The average water pressure thereby reaches up to 1.07 bar, compared to maximum values of 1.3 bar recorded by the submersible drifters.

4 Discussion and Conclusions

We showed the topological reconstruction of a supra-, as well as an englacial channel on Austre Brøggerbreen (Svalbard) and used these reconstructions to spatially reference the pressure distributions within these channels.

The results of the supraglacial channel show a progressively enhanced sequencing of meander bends in the lower part of the channel. Aligning the pressures to the reconstructed flow path reveals zones of larger pressure variations in the same section of the channel. This is in accordance with our previous work (Alexander, Kruusmaa, et al., 2020), where we showed the connection between larger pressure variations and morphological features in the channel, such as step-pool sequences and meander bends. Visual observations during the fieldwork of this study further confirm this connection, as several meander bends, as well as step-pool sequences, existed in the lower part. This is also in good agreement with the results of the topological reconstruction of the channel.

It is important to emphasize, that the GNSS reference used in the supraglacial channel reconstruction is not the most accurate. The static positioning error of the used GNSS receivers is ±3 m (Tuhtan et al., 2020), with the dynamic positioning error, in a highly turbulent supraglacial stream, certainly being higher. The used GNSS reference path is additionally an aligned average of 26 single tracks (Alexander et al., n.d.), thereby over-smoothing several meander-bends and therefore smoothing the real channel geometry. An average error of 3.90 m for the reconstruction versus the GNSS reference path is therefore likely below the accuracy of the GNSS reference track itself. The over-smoothing of the GNSS reference path also explains, why the reconstructed path's length is 6.5% longer compared to the GNSS reference. We therefore estimate the error of our reconstruction to be closer to the values calculated for the rectangular validation case, where a dGPS reference path was available.

The flow path of the englacial channel, investigated in this study, has been repeatedly mapped by previous studies. (Stuart et al., 2003) utilized GPR to draw a map of the channel (shown in fig. 1(c)), whereas (Vatne, 2001) used speleological investigations, providing a very simple map in his publication. These studies allow us to approximately assess the feasibility of our reconstructed flow path, as well as the evolution of the channel as both previous investigations took place twenty years earlier.

We have further revisited the englacial channel in late summer 2020. Heavy summer melt, in both 2019 and 2020, has led to the melt-out of the englacial channel, which by the end of 2020 was not longer an englacial channel, but rather a deeply incised canyon. This has allowed us to collect a GNSS reference path using a GNSS enabled drifter (Tuhtan et al., 2020; Alexander et al., n.d.) and further visually inspect parts of the channel. Both the 2020 GNSS reference path, the 1999 GPR reconstruction and our 2019 reconstruction are shown in figure 7(b).

The qualitative comparison between the 1999 GPR reconstruction of the englacial channel from (Stuart et al., 2003) and our GNSS surface drifter measurements from 2020 show good accordance in the overall shape of the flow path. It is visible that the channel developed by both vertical and lateral incision, thereby keeping its' overall shape over the 21 years spanning between the two investigations. Our 2019 reconstruction is well within this overall shape, reflecting the same qualitative flow path. The error of our reconstruction is 12.1 m, which is higher than the error of the supraglacial reconstruction. We assume that this is mainly due to the lack of an accurate reference path. The positional accuracy of the obtained 2020 GNSS path is likely much lower than in the supraglacial case, as the quality of the received GNSS signal in the up to 20 m deep, narrow and partly ice covered canyon was not the best. The used satellite reference for the canyon (fig. 1(f)) and the proglacial river (fig. 1(g)) was mapped on planet imagery, which have a positional accuracy of less than 10 m RMSE (Team Planet, 2017). The canyon was thereby barely visible on the imagery leading to a straight reference track instead of a meandering one, as the real geometry would have implied (see fig. 1(f)). We therefore attribute the higher calculated error of the englacial channel to the lower accuracy of the used reference paths compared to the validation cases.

The length of the flow path of the englacial reconstruction is 1027 m, much longer than the sum of the GNSS and the satellite reference path of 834.8 m. The GNSS reference path is, however, missing the first section of the englacial channel after deployment due to changed water pathways between 2019 and 2020. Based on handhold GPS measurements, this length difference is estimated to be 85 m. This leaves a difference of 107.2 m between reference track length and the reconstruction or an overestimation of the track by 11.4%. This does, however, not take into account that the satellite reference path is underestimating the real track length. Therefore the real length error of our reconstruction is likely much lower. On the other hand, the drifter based reconstruction could also overestimate the channel length. Our reconstruction is based on the distance travelled by the drifters. As they can get stuck in eddies or travel from one side of the channel to the other, the reconstructed path becomes longer than the real channel. This can also be seen in very wobbly sections of the channel reconstruction in figure 7(a).

The pressures recorded by the submersible drifters in the englacial channel show flow under atmospheric conditions. Pressurized flow conditions, where the water flows uphill as encountered by (Stuart et al., 2003), do not longer exist within the channel. The average error of the pressure data is, with 3.4 mbar, similar to our previous work (Alexander, Kruusmaa, et al., 2020), thus very low. Within the englacial channel itself, one zone of abrupt and high pressure change exists shortly before the channel exits into the canyon. Similar to pressure peaks studied in

(Alexander, Kruusmaa, et al., 2020), we interpret this as the presence of a step-pool sequence with a large step riser. This interpretation was confirmed by speleological investigations in 2018, where a roughly 2.5 m high step riser was found at the same location.

In this study we used a relatively low number of deployments (11 for the supraglacialchannel and 6 for the englacial channel) for the reconstruction with an average error of 3.90 m and 12.1 m, respectively. The average error calculations for the supraglacial channel (figure 6) show that the error converges at 6 deployments. The decrease of the average error with increasing deployment number is, however, so low (2.5%) that a single deployment would already lead to sufficient precision. Using the values for the mean pressure and its' standard deviation, leads to a precision of 0.66% with just one deployment, according to equation 4 in (Alexander, Kruusmaa, et al., 2020). This shows, that our approach is able to produce a highly precise topological reconstruction and spatial pressure distribution from just one deployment. As we have lost one submersible drifter out of 24 deployments at the englacial channel (95.8% recovery rate) and encountered technical problems (e.g. drifter switched off during deployment, damaged pressure recordings) with quite some of the retrieved datasets (utility rate of only 25%), we estimate that at least 5 submersible drifter deployments will be needed in the field in order to obtain the topology of an englacial channel.

At the current stage we are only able to produce the planar topology of the flow path. A full 3D reconstruction was not possible because the used IMUs (Alexander, Kruusmaa, et al., 2020) do not correct for the gravity vector. Removing the gravity vector in the post-processing stage introduces additional uncertainty and therefore renders an inaccurate elevation track. We are, however, optimistic that we will be able to do full 3D reconstructions in an improved version of our method, by collecting additional vertical reference data and accounting for the error introduced by the gravity vector. The current model is also not able to calculate the numerical velocity, as the model operates largely on a normalised space. Another development step will therefore be to also reconstruct flow velocities utilizing the time stamp of the IMU recordings alongside the reconstructed path length. Mapping flow velocities alongside pressure distribution would provide an additional input for numerical flow models.

Overall, we have developed a method that is able to produce decent flow path reconstructions with only two given coordinates. As our method can already be run with the data from just one submersible drifter deployment and on a consumer laptop, it will be practical for a variety of field applications. This suggests that our results might have larger implications, not only for glaciology, but also for subsurface flow studies in general.

4.1 Data archival

All data will be made publicly available at the end of the peer-review process.

Acknowledgments

The fieldwork for this project was funded by the H2020 INTERACT Transnational Access project DeepSense 2019, University of Oslo Industrial Liason, University of Oslo Garpen Stipend, the Department of Geosciences University of Oslo, the Research Council of Norway funded MAMMAMIA project (grant number 301837 MAMMAMIA: Multi-scale multi-method analysis of mechanisms causing ice acceleration) and the Svalbard Environmental protection fund (17/31). This research was further funded by the European Research Council (grant no. ICEMASS) and the Research Council of Norway (grant no. 223254 – NTNU AMOS). Fieldwork in

2020 was funded by the Research Council of Norway via an Arctic Field Grant to AA (Dynamics of glacial channels, RiS ID 11423). This study is a contribution to the Svalbard Integrated Arctic Earth Observating System (SIOS). We further on acknowledge support from the team of the NPI Sverdrup station, particularly Vera Sklet, during the fieldwork. Asko Ristolainen and Astrid Tesaker helped during the 2020 field campaign. The drifters used in this study were originally designed by Jeffrey A. Tuhtan and Juan Francisco Fuentes-Perez. We also acknowledge Jeffreys' contribution during the 2019 fieldwork for this study and his valuable input for model development and scientific discussions. The GNSS surface drifter figure was provided by Kerstin Alexander.

References

Alexander, A., Kruusmaa, M., Tuhtan, J. A., Hodson, A., Schuler, T., & Kääb, A. (2020). Pressure and inertia sensing drifters for glacial hydrology flow path measurements. *The Cryosphere*, *14*, 1009-1023.

Alexander, A., Obu, J., Schuler, T. V., Kääb, A., & Christiansen, H. H. (2020). Subglacial permafrost dynamics and erosion inside subglacial channels driven by surface events in svalbard. *The Cryosphere*, *14*(11), 4217–4231. Retrieved from `https://tc.copernicus.org/articles/14/4217/2020/` doi: 10.5194/tc-14-4217-2020

Alexander, A., Tuhtan, J., Kruusmaa, M., Schuler, T., & Kääb, A. (n.d.). Spatiotemporal distribution of water flow velocities, accelerations and ice melt rates inside a small supraglacial channel derived from drifter measurements. *In preparation*.

Andrews, L. C., Catania, G. A., Hoffman, M. J., Gulley, J. D., Lüthi, M. P., Ryser, C., ... Neumann, T. A. (2014). Direct observations of evolving subglacial drainage beneath the greenland ice sheet. *Nature*, *514*(7520), 80–83.

Bælum, K., & Benn, D. I. (2011). Thermal structure and drainage system of a small valley glacier (tellbreen, svalbard), investigated by ground penetrating radar. *The Cryosphere*, *5*(1), 139.

Bagshaw, E. A., Burrow, S., Wadham, J. L., Bowden, J., Lishman, B., Salter, M., ... Nienow, P. (2012). E-tracers: Development of a low cost wireless technique for exploring sub-surface hydrological systems. *Hydrological Processes*, *26*(20), 3157–3160.

Bagshaw, E. A., Lishman, B., Wadham, J. L., Bowden, J. A., Burrow, S. G., Clare, L. R., & Chandler, D. (2014). Novel wireless sensors for in situ measurement of sub-ice hydrologic systems. *Annals of glaciology*, *55*(65), 41–50.

Beal, M. J., Ghahramani, Z., & Rasmussen, C. E. (2002). The infinite hidden markov model. In *Advances in neural information processing systems* (pp. 577–584).

Björnsson, H. (1975). Subglacial water reservoirs, jökulhlaups and volcanic eruptions. *Jökull*, *25*, 1–14.

Engelhardt, H., Humphrey, N., Kamb, B., & Fahnestock, M. (1990). Physical conditions at the base of a fast moving antarctic ice stream. *Science*, *248*(4951), 57–59.

Flowers, G. E. (2015a). Modelling water flow under glaciers and ice sheets. *Proceedings of the Royal Society A: Mathematical, Physical and Engineering Sciences*, *471*(2176), 20140907.

Flowers, G. E. (2015b). Modelling water flow under glaciers and ice sheets. *Proceedings of the Royal Society A: Mathematical, Physical and Engineering Sciences*, *471*(2176), 20140907.

Fountain, A. G., & Walder, J. S. (1998). Water flow through temperate glaciers. *Reviews of Geophysics*, *36*(3), 299–328.

Fourati, H., Manamanni, N., Afilal, L., & Handrich, Y. (2013). Position estimation

approach by complementary filter-aided imu for indoor environment. In *2013 european control conference (ecc)* (pp. 4208–4213).

Gimbert, F., Tsai, V. C., Amundson, J. M., Bartholomaus, T. C., & Walter, J. I. (2016). Subseasonal changes observed in subglacial channel pressure, size, and sediment transport. *Geophysical Research Letters*, *43*(8), 3786–3794.

Gulley, J. D., Benn, D. I., Screaton, E., & Martin, J. (2009). Mechanisms of englacial conduit formation and their implications for subglacial recharge. *Quaternary Science Reviews*, *28*(19-20), 1984–1999.

Hansen, L. U., Piotrowski, J. A., Benn, D. I., & Sevestre, H. (2020). A cross-validated three-dimensional model of an englacial and subglacial drainage system in a high-arctic glacier. *Journal of Glaciology*, *66*(256), 278–290.

Holmlund, P. (1988). Internal geometry and evolution of moulins, storglaciären, sweden. *Journal of Glaciology*, *34*(117), 242–248.

Hooke, R. L. (1989). Englacial and subglacial hydrology: a qualitative review. *Arctic and Alpine Research*, *21*(3), 221–233.

Hubbard, B., & Nienow, P. (1997). Alpine subglacial hydrology. *Quaternary Science Reviews*, *16*(9), 939–955.

Hubbard, B., Sharp, M. J., Willis, I. C., Nielsen, M., & Smart, C. C. (1995). Borehole water-level variations and the structure of the subglacial hydrological system of haut glacier d'arolla, valais, switzerland. *Journal of Glaciology*, *41*(139), 572–583.

Iken, A. (1972). Measurements of water pressure in moulins as part of a movement study of the white glacier, axel heiberg island, northwest territories, canada. *Journal of Glaciology*, *11*(61), 53–58.

Iken, A., & Bindschadler, R. A. (1986). Combined measurements of subglacial water pressure and surface velocity of findelengletscher, switzerland: conclusions about drainage system and sliding mechanism. *Journal of Glaciology*, *32*(110), 101–119.

Kamintzis, J. E., Jones, J. P. P., Irvine-Fynn, T. D. L., Holt, T. O., Bunting, P., Jennings, S. J. A., ... Hubbard, B. (2018). Assessing the applicability of terrestrial laser scanning for mapping englacial conduits. *Journal of Glaciology*, *64*(243), 37–48.

Killick, R., Fearnhead, P., & Eckley, I. A. (2012). Optimal detection of changepoints with a linear computational cost. *Journal of the American Statistical Association*, *107*(500), 1590–1598.

Montello, D. R. (2005). *Navigation.* Cambridge University Press.

Nanni, U., Gimbert, F., Vincent, C., Gräff, D., Walter, F., Piard, L., & Moreau, L. (2020). Quantification of seasonal and diurnal dynamics of subglacial channels using seismic observations on an alpine glacier. *The Cryosphere*, *14*(5), 1475–1496.

Pörtner, H.-O., Roberts, D. C., Masson-Delmotte, V., Zhai, P., Tignor, M., Poloczanska, E., ... others (2019). Ipcc special report on the ocean and cryosphere in a changing climate. *IPCC Intergovernmental Panel on Climate Change (IPCC)*.

Röthlisberger, H. (1972). Water pressure in intra-and subglacial channels. *Journal of Glaciology*, *11*(62), 177–203.

Sakoe, H., & Chiba, S. (1978). Dynamic programming algorithm optimization for spoken word recognition. *IEEE transactions on acoustics, speech, and signal processing*, *26*(1), 43–49.

Savitzky, A., & Golay, M. J. E. (1964). Smoothing and differentiation of data by simplified least squares procedures. *Analytical chemistry*, *36*(8), 1627–1639.

Schaap, T., Roach, M. J., Peters, L. E., Cook, S., Kulessa, B., & Schoof, C. (2020). Englacial drainage structures in an east antarctic outlet glacier. *Journal of Glaciology*, *66*(255), 166–174.

Sethuraman, J. (1994). A constructive definition of dirichlet priors. *Statistica sinica*, 639–650.

Shreve, R. L. (1972). Movement of water in glaciers. *Journal of Glaciology*, *11*(62), 205–214.

Stone, D. B., & Clarke, G. K. C. (1996). In situ measurements of basal water quality and pressure as an indicator of the character of subglacial drainage systems. *Hydrological Processes*, *10*(4), 615–628.

Stuart, G., Murray, T., Gamble, N., Hayes, K., & Hodson, A. (2003). Characterization of englacial channels by ground-penetrating radar: An example from austre brøggerbreen, svalbard. *Journal of Geophysical Research: Solid Earth*, *108*(B11).

Team Planet. (2017). *Planet application program interface: In space for life on earth.* Retrieved from `https://api.planet.com`

Thrun, S. (1998). Learning metric-topological maps for indoor mobile robot navigation. *Artificial Intelligence*, *99*(1), 21–71.

Thrun, S., Burgard, W., & Fox, D. (1998). A probabilistic approach to concurrent mapping and localization for mobile robots. *Autonomous Robots*, *5*(3-4), 253–271.

Tuhtan, J., Alexander, A., Kruusmaa, M., & Fuentes-Pérez, J. (2020). Multiscale change detection in a supraglacial stream using surface drifters. In *Proceedings of the international conference on river flow 2020.* Delft.

Van Gael, J., Saatci, Y., Teh, Y. W., & Ghahramani, Z. (2008). Beam sampling for the infinite hidden markov model. In *Proceedings of the 25th international conference on machine learning* (pp. 1088–1095).

Vatne, G. (2001). Geometry of englacial water conduits, austre brøggerbreen, svalbard. *Norsk Geografisk Tidsskrift*, *55*(2), 85–93.

Vatne, G., & Irvine-Fynn, T. (2016). Morphological dynamics of an englacial channel. *Hydrology and Earth System Sciences*, *20*(7), 2947–2964.

Vieli, A., Jania, J., Blatter, H., & Funk, M. (2004). Short-term velocity variations on hansbreen, a tidewater glacier in spitsbergen. *Journal of Glaciology*, *50*(170), 389–398.